Science of the Total Environment 875 (2023) 162586

Contents lists available at ScienceDirect

Science of the Total Environment

journal homepage: www.elsevier.com/locate/scitotenv

Tim4, a macrophage receptor for apoptotic cells, binds polystyrene microplastics via aromatic-aromatic interactions

Miki Kuroiwa [a,1], Shin-Ichiro Yamaguchi [a,1], Yoshinobu Kato [a], Arisa Hori [a], Saori Toyoura [a], Mai Nakahara [a], Nobuyuki Morimoto [b], Masafumi Nakayama [a,*]

[a] Laboratory of Immunology and Microbiology, College of Pharmaceutical Sciences, Ritsumeikan University, Kusatsu, Japan
[b] Department of Materials for Energy, Shimane University, Shimane, Japan

HIGHLIGHTS

- Tim4 binds polystyrene (PS) microplastics via aromatic-aromatic interactions.
- Tim4 is involved in macrophage engulfment of PS microplastics.
- PS microplastics do not stimulate macrophages to produce inflammatory cytokines.
- PS microplastics perturb Tim4-mediated efferocytosis.

GRAPHICAL ABSTRACT

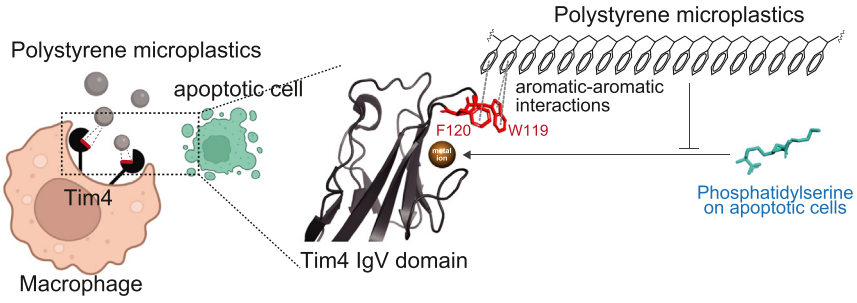

ARTICLE INFO

Editor: Jay Gan

Keywords:
Microplastics
Polystyrene
Macrophage
Phagocytosis
Scavenger receptor

ABSTRACT

Understanding the interface between microplastics and biological systems will provide new insights into the impacts of microplastics on living organisms. When microplastics enter the body, they are engulfed preferentially by phagocytes such as macrophages. However, it is not fully understood how phagocytes recognize microplastics and how microplastics impact phagocyte functions. In this study, we demonstrate that T cell immunoglobulin mucin 4 (Tim4), a macrophage receptor for phosphatidylserine (PtdSer) on apoptotic cells, binds polystyrene (PS) microparticles as well as multi-walled carbon nanotubes (MWCNTs) through the extracellular aromatic cluster, revealing a novel interface between microplastics and biological systems via aromatic-aromatic interactions. Genetic deletion of Tim4 demonstrated that Tim4 is involved in macrophage engulfment of PS microplastics as well as of MWCNTs. While Tim4-mediated engulfment of MWCNTs causes NLRP3-dependent IL-1β secretion, that of PS microparticles does not. PS microparticles neither induce TNF-α, reactive oxygen species, nor nitric oxide production. These data indicate that PS microparticles are not inflammatory. The PtdSer-binding site of Tim4 contains an aromatic cluster that binds PS, and Tim4-mediated macrophage engulfment of apoptotic cells, a process called *efferocytosis*, was competitively blocked by PS microparticles. These data suggest that PS microplastics do not directly cause acute inflammation but perturb efferocytosis, raising concerns that chronic exposure to large amounts of PS microplastics may cause chronic inflammation leading to autoimmune diseases.

1. Introduction

Global production of plastics is estimated to be 400 million tons per year, approximately half of which is used as single-use packaging, thus resulting in plastic waste (MacLeod et al., 2021; Wright and Kelly, 2017). In the environment, most plastics are not biodegradable and become brittle

* Corresponding author at: Laboratory of Immunology and Microbiology, College of Pharmaceutical Sciences, Ritsumeikan University, 1-1-1 Noji-Higashi, Kusatsu, Shiga 525-8577, Japan.
E-mail address: mnakayam@fc.ritsumei.ac.jp (M. Nakayama).
[1] Contributed equally.

http://dx.doi.org/10.1016/j.scitotenv.2023.162586
Received 12 December 2022; Received in revised form 21 February 2023; Accepted 27 February 2023
Available online 3 March 2023

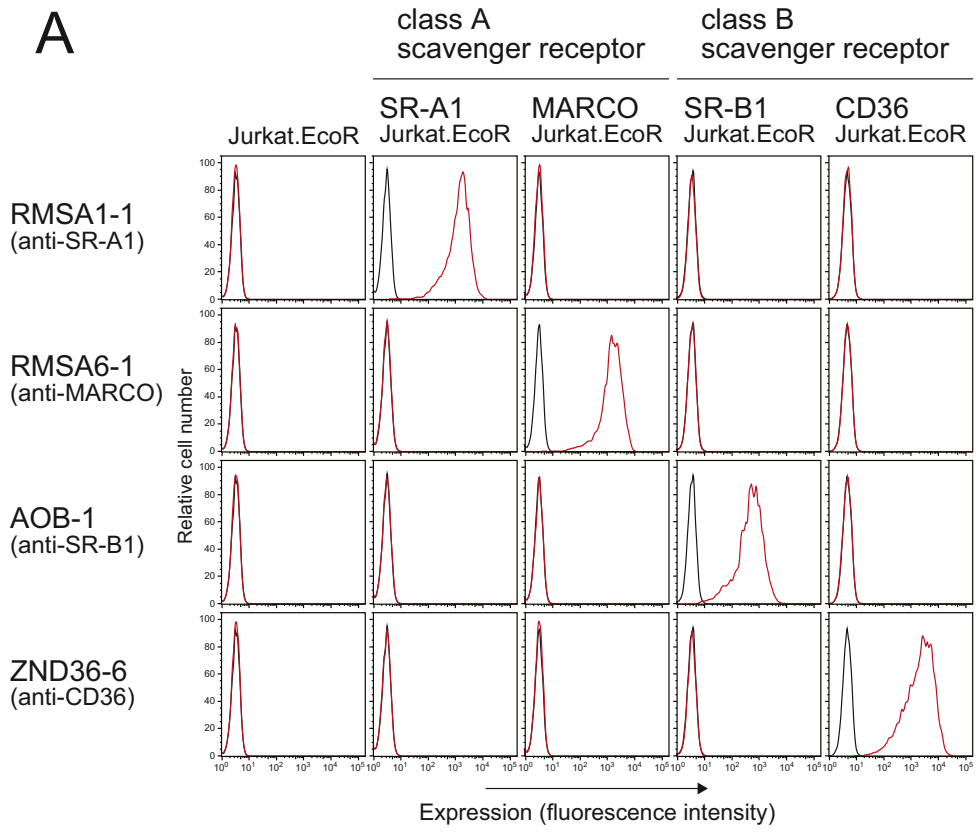
A
class A scavenger receptor
class B scavenger receptor
SR-A1
MARCO
SR-B1
CD36
Jurkat.EcoR
RMSA1-1 (anti-SR-A1)
RMSA6-1 (anti-MARCO)
AOB-1 (anti-SR-B1)
ZND36-6 (anti-CD36)
Relative cell number
Expression (fluorescence intensity)

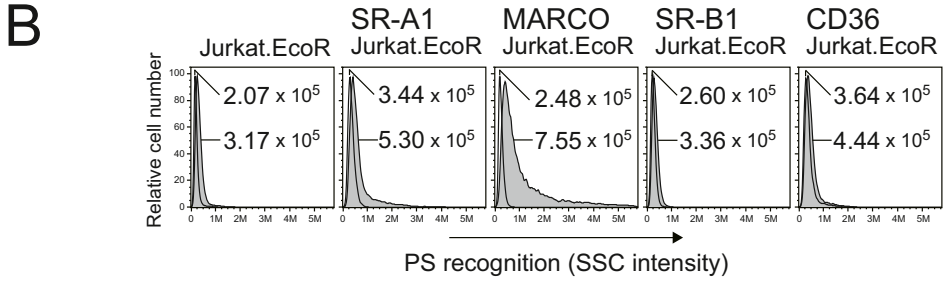
B
Jurkat.EcoR
SR-A1
MARCO
SR-B1
CD36
2.07 x 10^5
3.17 x 10^5
3.44 x 10^5
5.30 x 10^5
2.48 x 10^5
7.55 x 10^5
2.60 x 10^5
3.36 x 10^5
3.64 x 10^5
4.44 x 10^5
Relative cell number
PS recognition (SSC intensity)

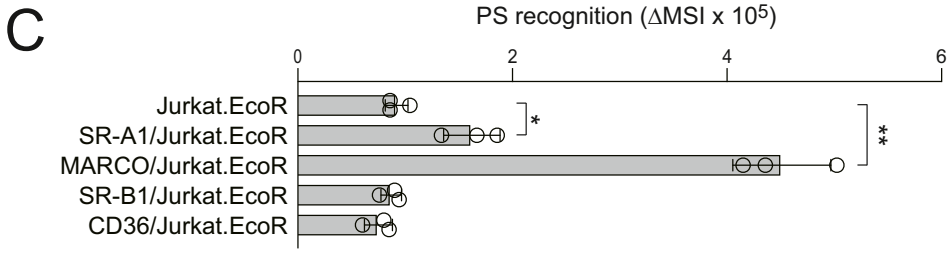
C
PS recognition (ΔMSI x 10^5)
Jurkat.EcoR
SR-A1/Jurkat.EcoR
MARCO/Jurkat.EcoR
SR-B1/Jurkat.EcoR
CD36/Jurkat.EcoR
*
**

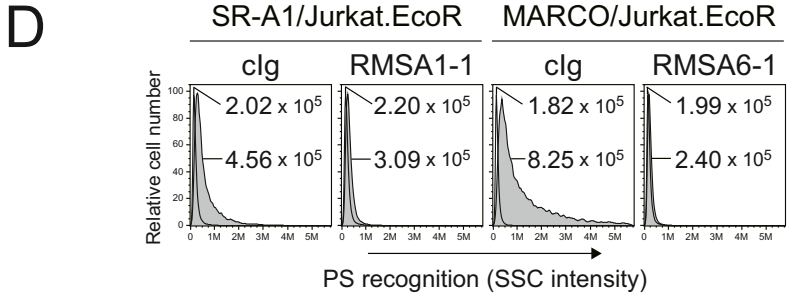
D
SR-A1/Jurkat.EcoR
MARCO/Jurkat.EcoR
cIg
RMSA1-1
cIg
RMSA6-1
2.02 x 10^5
4.56 x 10^5
2.20 x 10^5
3.09 x 10^5
1.82 x 10^5
8.25 x 10^5
1.99 x 10^5
2.40 x 10^5
Relative cell number
PS recognition (SSC intensity)

due to ultraviolet exposure, resulting in their fragmentation into microplastics (0.1–1000 μm size) (Cozar et al., 2014; Koelmans et al., 2022). These microplastics are ubiquitous, some of which may eventually enter the human food chain and others of which may exist atmospherically (MacLeod et al., 2021; Mitrano et al., 2021; Stubbins et al., 2021). Thus, humans are likely exposed to microplastics not only via diet, but also via inhalation (Amato-Lourenco et al., 2020; Wright and Kelly, 2017). Indeed, recent studies have detected microplastics in human blood and organs (Horvatits et al., 2022; Leslie et al., 2022). Although plastics have been considered to be bioinert, which is one reason they are widely used, it remains unknown whether chronic exposure to microplastics impacts human health (Vethaak and Legler, 2021). Upon entering into living organisms, microplastics are efficiently engulfed by phagocytes such as macrophages (Prata, 2018; Prata et al., 2020; Shi et al., 2022; Wright and Kelly, 2017). However, it is not well understood how macrophages recognize microplastics and whether microplastics impact macrophage functions.

Under physiological conditions, macrophages play an important role in efferocytosis to prevent inflammation and autoimmune diseases (Doran et al., 2020; Nagata, 2018). On the other hand, when environmental particles enter the body, macrophages also engulf these inorganic particles and could provoke inflammation (Heppleston, 1984; Leung et al., 2012). For instance, upon being engulfed, silica, asbestos, and carbon nanotubes (CNTs) are not digested in phagosomes and instead cause phagosome damage, which activates the NLRP3 inflammasome and IL-1β processing, provoking inflammation (Franklin et al., 2016; Rashidi et al., 2020; Swanson et al., 2019). Compared with these particles and fibers, microplastics are considered to be non-inflammatory and bioinert (Andrady, 2011). However, some microplastics have recently been reported to induce macrophage activation (Jeon et al., 2021; Merkley et al., 2022). In addition, it has been hypothesized that phagocytes engulfing microplastics may convey them into various organs, causing organ dysfunction (Ramsperger et al., 2020; Wright and Kelly, 2017). In this context, it is important to understand how macrophages recognize microplastics. The class A scavenger receptor, macrophage receptor with collagenous structure (MARCO) (also known as SR-A6), reportedly binds polystyrene (PS) (Arredouani et al., 2004; Kanno et al., 2007), one of the major types of plastic debris accumulated in the environment (Jang et al., 2017; Stubbins et al., 2021); however, it remains unknown whether MARCO is essential for the recognition of PS microplastics by macrophages. Furthermore, other scavenger receptors (Areschoug and Gordon, 2009) may also be involved in this process.

We have recently demonstrated that a phosphatidylserine (PtdSer) receptor, T cell mucin immunoglobulin 4 (Tim4) (Miyanishi et al., 2007), also works as a receptor for CNTs (Omori et al., 2021). While Tim4 plays an essential role for efferocytosis (Miyanishi et al., 2007; Nagata, 2018), it also mediates phagocytosis of multi-walled CNTs (MWCNTs), leading to NLRP3 inflammasome activation and IL-1β processing, provoking inflammation (Omori et al., 2021). It is noteworthy that Tim4 has a unique aromatic cluster in its extracellular loop, which is essential for aromatic-aromatic interactions between Tim4 and the carbon nanomaterial surface (Omori et al., 2021). This finding prompted us to address whether Tim4 also binds PS, which consist of aromatic hydrocarbon styrene. Here we investigate the role of Tim4 in macrophage recognition of PS microplastics.

2. Materials and methods

2.1. Characterization of particles

Mean diameter 0.8 μm (LB8), 0.1 μm PS (LB1) PS microspheres, and diameter × length 110–170 nm × 5–9 μm MWCNTs (659258) were all purchased from Sigma-Aldrich. Diameter 0.2–9.9 μm Polyethylene (PE) microspheres (PENS-0.95) were purchased from Cospheric. These particle sizes are supplied by manufactures. PS particles were sputter-coated with platinum using an ion coaster (JEC-3000FC, JEOL) and were observed by scanning electron microscopy (SEM; JSM-7900F, JEOL). The obtained SEM images were analyzed the particle size using ImageJ software ver. 1.46r. The hydrodynamic diameter and the zeta potential of the PS particles were analyzed by a Zetasizer Ultra instrument (Malvern Instruments, Malvern, U.K.) equipped with a PELTIER temperature control unit at a wavelength of 632.8 nm and a 173°detection angle. The PS particle (0.1 mg/ml) was dispersed in phosphate-buffered saline (PBS), and the dispersion was then sonicated in an ultrasonic bath at 28 kHz and 100 W for 10 min. The dispersions were equilibrated at 37 °C for 30 min before the measurements. The hydrodynamic diameter and the zeta potential were calculated from the obtained data using software from the supplier, ZS XSPLORER ver. 3.2.1.11.

2.2. Mice and peritoneal resident cells

C57BL/6 J (B6) mice were obtained from CLEA Japan. Tim4 knockout (KO) mice (Miyanishi et al., 2012) were kindly provided by Professor Shigekazu Nagata (Osaka University). Nlrp3 KO mice (Kovarova et al., 2012) were obtained from The Jackson Laboratory. All mice were maintained in specific pathogen-free conditions according to the Guidelines for Proper Conduct of Animal Experiments (Science Council of Japan). Mouse peritoneal resident cells were harvested with cold sterile PBS containing 1 mM EDTA. Cell population was analyzed by an Accuri C6 cytometer (BD Biosciences) using fluorescein isothiocyanate (FITC)-anti-CD3 mAb (BioLegend), Phycoerythrin (PE)-anti-CD11b, PerCP/Cyanine5.5-anti-CD19 (BioLegend), and Allophycocyanin (APC)-anti-NK1.1 mAb (BioLegend). Total 10,000 cells per sample were recorded. All protocols were approved by the Institutional Animal Care and Use Committee (IACUC) of Ritsumeikan University (Approved number: BKC2019-030) and Shiga University School of Medicine (Approved number: 2022-6-12).

2.3. Cell lines

Jurkat.EcoR cells (Tsugita et al., 2017) were maintained in complete RPMI (RPMI supplemented with 10 % FBS, 100 U/ml penicillin, 100 μg/ml streptomycin, 2 mM glutamine, and 1 mM sodium pyruvate). NIH-3T3 cells (American Type Culture Collection [ATCC]) were maintained in complete DMEM. The coding regions of mouse SR-A1 (GeneBank: NM_031195.2) and MARCO (GeneBank: NM_010766.3) were amplified from B6 mouse bone marrow-derived macrophages and splenic dendritic cells, respectively. These cDNAs were subcloned into pMX-IP (Kitamura et al., 2003) and retrovirally transduced into Jurkat.EcoR cells and NIH-3T3 cells. SR-B1/Jurkat.EcoR cells, CD36/Jurkat.EcoR cells, Tim4/NIH-3T3 cells, and Tim4 WF119/120AA mutant/NIH-3T3 cells were generated previously (Omori et al., 2021; Tsugita et al., 2017).

Fig. 1. Generation of mouse class A scavenger receptor transfectants and their mAbs. A. Indicated Jurkat.EcoR cells were stained with biotinylated control rat IgG2a (cIg: black histograms) or indicated anti-scavenger receptor mAbs (red histograms), followed by streptavidin-phycoerythrin (PE). The specificity of each mAb was analyzed by flow cytometry. B. Indicated Jurkat.EcoR cells were treated with (dark histograms) or without (white histograms) 100 μg/ml of 0.8 μm diameter polystyrene (PS) particles for 30 min. PS binding was analyzed by flow cytometry. Numbers indicate the median side scatter intensity (MSI). See also Fig. S1. C. PS recognition was analyzed as in B. The delta median side scatter intensity (ΔMSI) was calculated by subtracting MSI of PS-treated cells from MSI of untreated cells in B. Data are shown as individual value (dots), mean (columns), and SD (error bars) from $n = 3$. *$p < 0.05$, **$p < 0.01$, one-way ANOVA. D. Indicated cells were pretreated with indicated mAb (10 μg/ml each) for 30 min and then were treated with 100 μg/ml of 0.8 μm PS particles for 30 min. PS binding was analyzed as in B. (For interpretation of the references to color in this figure legend, the reader is referred to the web version of this article.)

2.4. Generation of mAbs

Anti-mouse SR-A1 mAb RMSA1-1 (rat IgG2a, κ) and anti-mouse MARCO mAb RMSA6-1 (rat IgG2a, κ) were generated according to our protocol (Tsugita et al., 2017) by which anti-mouse SR-B1 mAb AOB-1 (rat IgG2a, κ) and anti-mouse CD36 mAb ZND36-6 (rat IgG2a, κ) had been generated. In brief, SD rats (CLEA Japan) were immunized subcutaneously in the footpad with SR-A1/NIH-3T3 or MARCO/NIH-3T3 cells emulsified in TiterMax Gold adjuvant (Sigma-Aldrich). Ten days later, rats were again immunized with SR-A1/NIH-3T3 or MARCO/NIH-3T3 cells, respectively, without adjuvant. Three days after this, rat popliteal lymph node cells were fused with P3U1 myeloma cells. After HAT (hypoxanthine-aminopterin-thymidine) selection, hybridoma cells were screened for the production of mAbs that bind to SR-A1 or MARCO.

2.5. Assessment of cell surface expression of macrophage receptors

Regarding scavenger receptor expression, cells were stained with biotinylated control rat IgG2a (cIg), RMSA1-1, RMSA6-1, AOB-1, or ZND36-6 (Tsugita et al., 2017) followed by streptavidin-phycoerythrin (PE) (BioLegend). Regarding Tim4 expression, cells were stained with PE-labeled cIg, or RMT4-54 (anti-Tim4: BioLegend). Mouse peritoneal resident cells were pretreated with clone 93 (anti-CD16/32: BioLegend) to block Fc receptors, and then stained with FITC-anti-CD11b (BioLegend) and the above mAbs. These cells were analyzed by an Accuri C6 cytometer (BD Biosciences). A minimum total 5,000 cells per sample were recorded.

2.6. Assessment of particle recognition by cells

The recognition of unlabeled particles by cells was assessed by flow cytometry as reported previously (Omori et al., 2021; Tsugita et al., 2017). In brief, NIH-3T3 cells (2.5×10^4/well) were seeded in 48-well plates and cultured overnight. Jurkat.EcoR cells and mouse peritoneal resident cells (1×10^5) were cultured in microtubes. These cells were incubated with the indicated concentration of particles for 30 min at 37 °C. After incubation with particles, cells were washed twice with PBS and then harvested. Mouse peritoneal resident cells were stained with FITC-anti-CD11b mAb and analyzed. In some assays, cells were pretreated with mAb 30 min before particle addition. Recognition of particles was analyzed by measuring side scatter (SSC) intensity on an Accuri C6 cytometer (BD Biosciences). A minimum total 5,000 cells per sample were recorded. For fluorescence microscopy, 4 % paraformaldehyde (Fujifilm)-fixed cells were permeabilized with 0.05 % Triton X (Sigma-Aldrich) and then were stained with Alexa fluor (AF) 594-Phalloidin (Thermo Fischer Scientific) and DAPI (Sigma-Aldrich) to visualize cell and nucleus morphology. Cells were then analyzed using the optical sectioning microscope BZ-X800 (KEYENCE) equipped with a 100× objective lens. For all studies, the recognition of particles by cells was synchronized by brief centrifugation (for 1 min at 400 ×*g*) of particles onto cells.

2.7. Measurement of cytokine production

IL-1β production was measured as reported previously (Omori et al., 2021). In brief, mouse peritoneal cells were primed with the indicated concentration of ultra-pure lipopolysaccharide (LPS; List Biological Lab) for 3 h and then stimulated with indicated concentration of particles or 10 μg/ml of Nigericin (Wako Pure Chemicals) for 4 h at 37 °C. Mouse IL-1β was measured in cell-culture supernatants (sup.) by ELISA (R&D) according to the manufacturer's instruction. Likewise, mouse TNF-α, IL-6, and IL-10 were also measured by ELISA (R&D).

2.8. Measurement of nitric oxide (NO) production

Mouse peritoneal resident cells (1.0×10^5/well) were seeded in 96 well half-area plate and then stimulated with particles (100 μg/ml) or IFN-γ (5 ng/ml; BioLegend) for 24 h at 37 °C. NO production was measured by Griess reagent kit (Dojindo) in cell culture supernatants according to the manufacture's instruction.

2.9. Measurement of reactive oxygen species (ROS) production

Mouse peritoneal resident cells (2.0×10^5/well) were primed with LPS (3 ng/ml) in 96-well plate for 4 h at 37 °C. These cells were stimulated with particles in the presence of dihydrorhodamine (DHR) 123 (1 μM; Sigma-Aldrich) for 2 h at 37 °C. After stimulation with particles, these cells were harvested and stained with Allophycocyanin (APC)-anti-CD11b mAb (BioLegend). The percent of DHR123-positice cells in CD11b-high macrophages were analyzed by an Accuri C6 cytometer (BD Biosciences). A minimum total 10,000 cells per sample were recorded.

2.10. Measurement of efferocytosis

Efferocytosis was analyzed as reported previously (Nakayama et al., 2009) with minor modifications. In brief, B6 mouse thymocytes were UV irradiated (100 mJ/cm^2) and then labeled with 1 μM CypHer5E, a pH-sensitive cyanine dye derivative (Cytiva). Mouse peritoneal resident cells (2×10^5/well) were cultured with CypHer5E-labeled apoptotic cells (1×10^6/well) in a 96-well plate for 30 min at 37 °C. Then cells were harvested and stained with FITC-anti-CD11b mAb. CypHer5E fluorescence intensity of CD11b-high macrophages was analyzed by an Accuri C6 cytometer (BD Biosciences). A minimum total 5,000 cells per sample were recorded. To address the effect of PS particles on the efferocytosis, peritoneal resident cells were pretreated with the indicated concentration of these particles 30 min before treatment of apoptotic cells.

2.11. Statistical analysis

All quantitative data collected from experiments is represented as the mean ± SD as indicated in the figure legends. Statistical analyses were performed using one- or two-way ANOVA: $*p < 0.05$; $**p < 0.01$.

3. Results

3.1. Scavenger receptor recognition of PS microplastics

To address the function of class A scavenger receptors in recognition of PS, we generated a lymphoma cell line, Jurkat.EcoR cells stably expressing mouse SR-A1 (also known as MSR1 or CD204) or MARCO (also known as SR-A6). Using these transfectants, we further generated anti-mouse SR-A1 mAb RMSA1-1 (rat IgG2a) and anti-mouse MARCO mAb RMSA6-1 (rat IgG2a) (Fig. 1A). We have previously generated anti-class B scavenger receptor mAbs: anti-mouse SR-B1 mAb, AOB-1 (rat IgG2a) and anti-mouse CD36 mAb, ZND36-6 (rat IgG2a) (Tsugita et al., 2017), and these four mAbs do not cross-react with other scavenger receptors (Fig. 1A). We next addressed whether these scavenger receptors bind PS microplastics. To this end, we used 0.8 μm diameter (supplied by the manufacture) particles, as this size of particles are considered to be easily inhaled and internalized by cells (Mitrano et al., 2021). Because cells recognizing crystalline particles exhibit the strong SSC intensity (Omori et al., 2021; Tsugita et al., 2017), we utilized this property to address the binding activity of cells to unlabeled particles. Among these scavenger receptors, MARCO expression markedly enabled Jurkat.EcoR cells to bind PS particles (Fig. 1B, C), which is consistent with previous reports (Arredouani et al., 2004; Kanno et al., 2007). The expression of SR-A1 also caused a slight increase, an effect not seen following the expression of SR-B1 or CD36 (Fig. 1B, C). The binding of PS particles to Jurkat.EcoR cells expressing MARCO or SR-A1 was confirmed by microscopy (Fig. S1). Further, we found that RMSA1-1 and RMSA6-1 completely blocked the binding of PS particles to SR-A1 and MARCO, respectively (Fig. 1D). These results suggest that class A scavenger receptors SR-A1 and MARCO, but not class B scavenger receptors SR-B1 and CD36, recognize PS particles.

We next addressed whether the class A scavenger receptors are involved in the recognition of PS particles by mouse peritoneal resident macrophages. These macrophages express both SR-A1 and MARCO on their cell surface (Fig. 2A) and efficiently recognize PS particles (Fig. 2B). However, unexpectedly, the blocking effect of RMSA6-1 was only partial and RMSA1-1 had no effect (Fig. 2B, C), suggesting the existence of class A scavenger receptor-independent pathways for the recognition of PS microplastics by macrophages.

3.2. Tim4 recognition of PS microplastics

To address whether Tim4 binds particles consisting of aromatic hydrocarbon styrene (Fig. 3A), we next used a fibroblast cell line, NIH-3T3 cells, stably expressing Tim4 (Fig. 3B) (Omori et al., 2021). As observed in the CNT binding assay (Omori et al., 2021), the expression of Tim4 enabled these cells to bind PS microparticles as well as MWCNTs, and the binding was completely abolished by replacement of both Trp119 and Phe120 with alanine residues (Fig. 3C, D, E). This suggests that aromatic-aromatic interactions between Tim4 and PS particles are essential for binding, which occurs in the same manner as CNT recognition.

We also used polyethylene (PE) particles. However, PE particles showed unsinkable property because of its specific gravity of 0.94 (Guo and Zhao, 2004) and rarely contacted adherent NIH-3T3 cells even after centrifugation (Fig. S2). Thus, we could not address whether Tim4 recognizes PE particles.

We then addressed whether Tim4 recognizes different sizes of PS particles. Besides 0.8 μm diameter PS particles that were used in all above experiments, 0.1 μm diameter PS particles were also used. As these particle sizes are supplied by the manufacture, we confirmed the size difference of these PS by SEM analysis (Fig. 4A). Both well-sized PS particles had smooth surfaces and spherical shapes. Calculated from the images, the size of 0.1 μm PS and 0.8 μm PS were indeed 78.4 ± 13.0 nm and 808.0 ± 35.1 nm, respectively. Further, we determined the hydrodynamic diameter and the distribution by dynamic light scattering measurements (Fig. 4B). The hydrodynamic diameter of 0.1 μm PS and 0.8 μm PS were 114.9 ± 5.3 nm and 1033.0 ± 32.2 nm, respectively. The average polydispersity index of the measurements was 0.063 (0.1 μm PS) and 0.149 (0.8 μm PS). Zeta potential was also measured in the same dispersion solution conditions. In the measurements, there was no significant difference between 0.1 μm PS (−37.4 ± 7.4) and 0.8 μm PS (−38.4 ± 3.8 mV) (Fig. 4B and Table 1).

We next addressed whether Tim4 is indeed involved in recognition of these PS particles by macrophages. To this end, we used mouse peritoneal resident cells that consist of lymphocytes ($CD3^+$ T cells, $CD19^+$ B cells, $NK1.1^+$ NK cells) and CD11b-high macrophages. Tim4 is highly expressed on macrophages but not on lymphocytes (Fig. S3). The loss of Tim4 expression was confirmed on macrophages from Tim4 KO mice (Fig. 5A). Although SSC intensity of 0.1 μm particles was lower than that of 0.8 μm particles, macrophages recognition of 0.1 μm particles was observed via flow cytometry (Fig. 5B). Importantly, Tim4 KO macrophages showed impaired binding to both sizes of PS particles (Fig. 5B, C). On the other hand, lymphocytes rarely recognized both sizes of particles (Fig. 5B, C). Taken together, these results indicate that Tim4 is involved in macrophage recognition of both sizes of PS particles.

We next addressed whether PS particles induce IL-1β secretion. To this end, we primed macrophages with 3 ng/ml of ultra-pure LPS, which is optimal concentration for macrophage priming to produce pro-IL-1β (Tsugita et al., 2017), and then stimulated cells with particles. Consistent with our recent paper (Omori et al., 2021), engulfment of MWCNTs by macrophages induced marked IL-1β secretion, which was impaired in Tim4 KO mouse macrophages and was completely abolished in NLRP3 KO mouse macrophages (Fig. 6). These results suggest that Tim4 is involved in engulfment of MWCNTs by macrophages and that NLRP3 (Franklin et al., 2016; Rashidi et al., 2020; Swanson et al., 2019) is essential for this fibre-induced IL-1β secretion. On the other hand, large amounts (100 μg/ml) of 0.8 μm PS particles induced only negligible IL-1β secretion, and 0.1 μm PS particles did not induce IL-1β at all (Fig. 6). We further used high-concentration (up to 200 ng/ml) of the LPS for the priming; however,

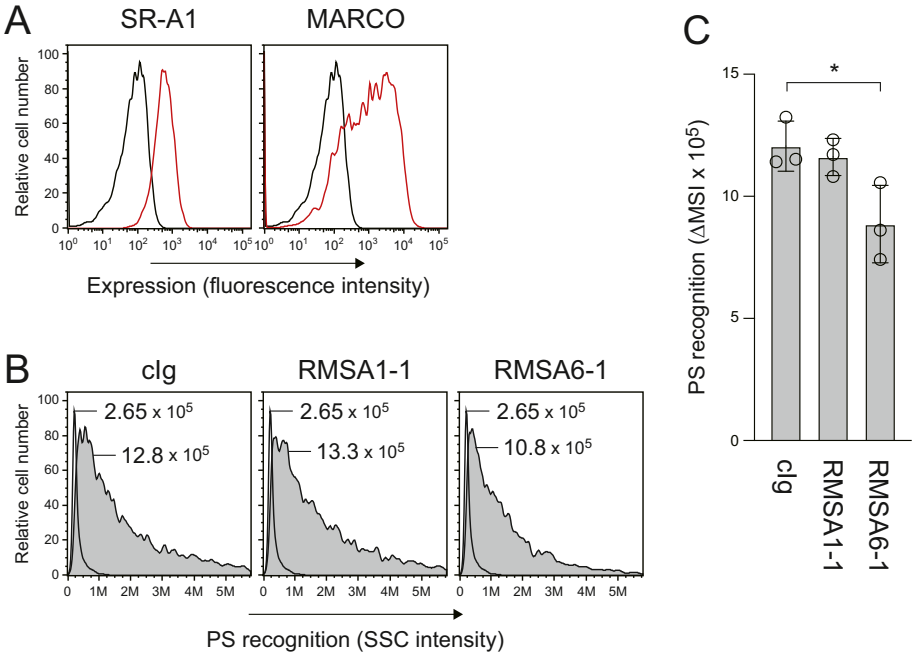

Fig. 2. Involvement of MARCO in macrophage recognition of PS microplastics. A. Mouse peritoneal resident cells were stained with FITC-anti-CD11b and biotinylated cIg (black histograms), RMSA1-1, or RMSA6-1 (red histograms), followed by streptavidin-PE. Cell surface expression of SR-A1 and MARCO on CD11b-high macrophages was analyzed by flow cytometry. B. Mouse peritoneal resident cells were pretreated with indicated mAb (10 μg/ml each) for 30 min and then were treated with 100 μg/ml of 0.8 μm PS for 60 min. Then cells were stained with FITC-anti-CD11b and analyzed by flow cytometry. Dark histograms indicate PS recognition by CD11b-high macrophages. White histograms indicate untreated macrophages. Numbers indicate MSI. C. PS recognition was analyzed as in B. The ΔMSI was calculated as in Fig. 1C. Data are shown as individual value (dots), mean (columns), and SD. (Error bars) from $n = 3$. *$p < 0.05$, one-way ANOVA. (For interpretation of the references to color in this figure legend, the reader is referred to the web version of this article.)

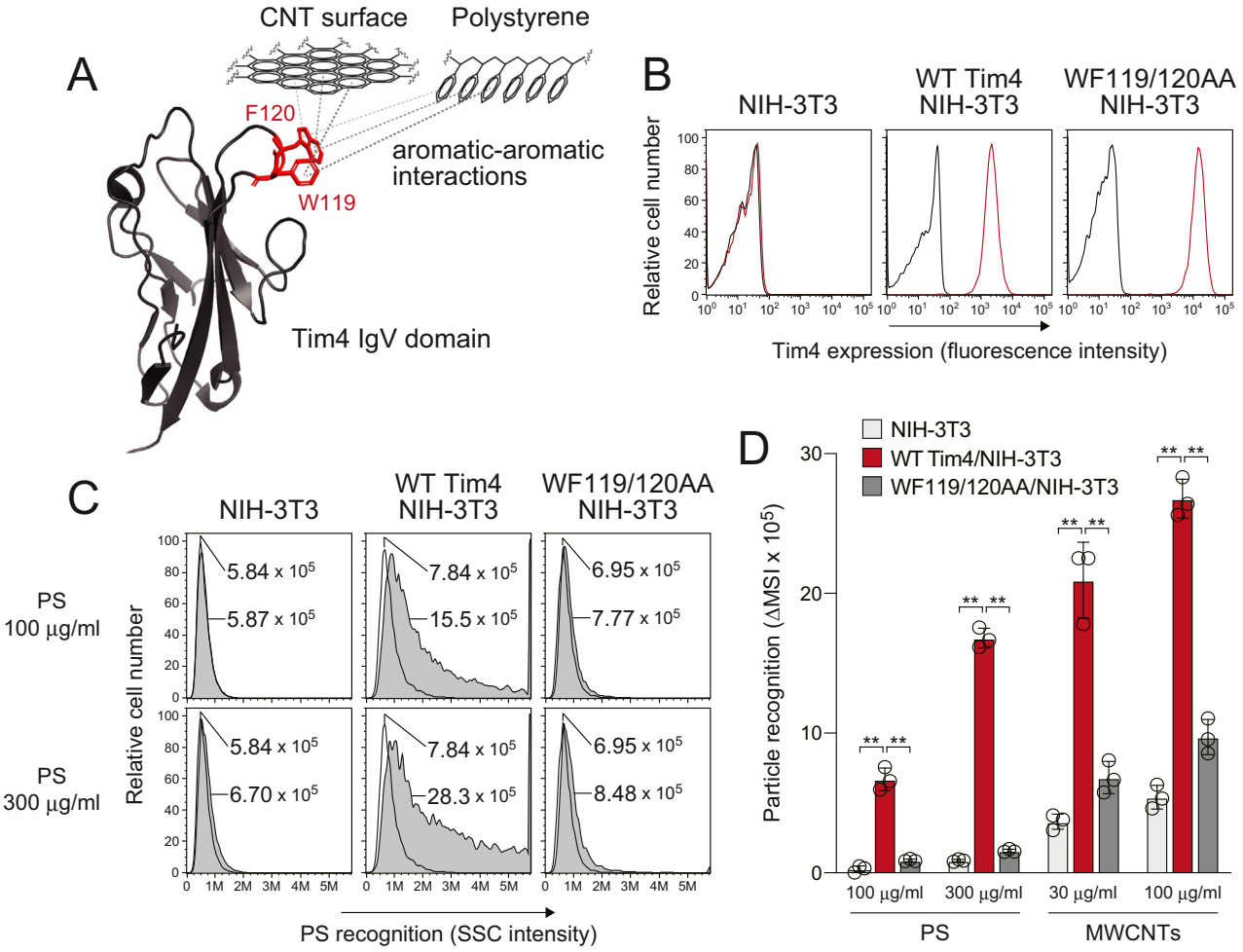
A
CNT surface
Polystyrene
F120
W119
aromatic-aromatic interactions
Tim4 IgV domain
B
NIH-3T3
WT Tim4 NIH-3T3
WF119/120AA NIH-3T3
Relative cell number
Tim4 expression (fluorescence intensity)
C
NIH-3T3
WT Tim4 NIH-3T3
WF119/120AA NIH-3T3
PS 100 μg/ml
PS 300 μg/ml
Relative cell number
5.84 x 10^5
5.87 x 10^5
7.84 x 10^5
15.5 x 10^5
6.95 x 10^5
7.77 x 10^5
5.84 x 10^5
6.70 x 10^5
7.84 x 10^5
28.3 x 10^5
6.95 x 10^5
8.48 x 10^5
PS recognition (SSC intensity)
D
NIH-3T3
WT Tim4/NIH-3T3
WF119/120AA/NIH-3T3
Particle recognition (ΔMSI x 10^5)
100 μg/ml
300 μg/ml
30 μg/ml
100 μg/ml
PS
MWCNTs
E
no particle
PS 100 μg/ml
NIH-3T3
WT Tim4 NIH-3T3
WF119/120AA NIH-3T3
Phalloidin
DAPI
BF
Merge

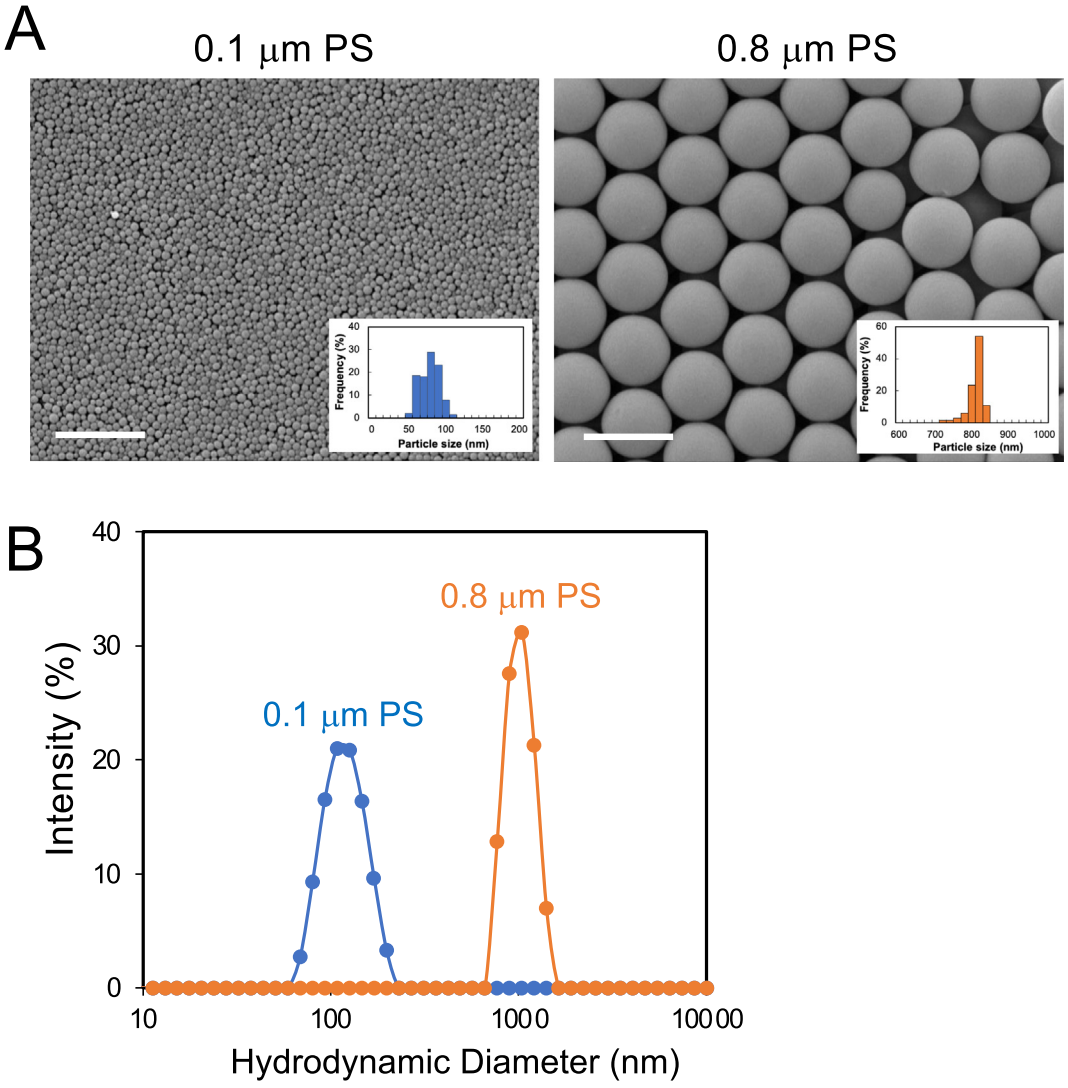

Fig. 4. Characterization of PS particles. A. Size and shape of PS particles were analyzed by scanning electron microscopy (SEM). White bars indicate 1 μm. The size and distribution of PS particles were calculated from SEM images and shown in inset graphs. B. Hydrodynamic diameter of PS particles in PBS (pH 7.4) was measured by dynamic light scattering.

Table 1
Characterization of PS particles.

Sample	Diameter (nm)		ζ-Potential (mV)
	$D_{(SEM)}$	$D_{(DLS)}$	
0.1 μm PS	78.4 ± 13.0	114.9 ± 5.3	−37.4 ± 7.4
0.8 μm PS	808.0 ± 35.1	1033.0 ± 32.2	−38.4 ± 3.8

these primed macrophages did not produce IL-1β in response to both sizes of PS (Fig. S4). TNF-α, IL-6, and IL-10 were secreted from macrophages stimulated with LPS alone, and PS did not affect these cytokine productions (Fig. S4).

To address whether Tim4 ligation by particles inhibits LPS-induced cytokine production, we next primed macrophages with LPS and particles simultaneously, and then stimulated these macrophages with Nigericin, a potassium ionophore that strongly induces NLRP3 inflammasome activation (Swanson et al., 2019). The Nigericin-induced IL-1β secretion was not affected by PS nor MWCNTs (Fig. S5). LPS-induced TNF-α production neither affected by PS nor MWCNTs (Fig. S5). These results suggest that Tim4 ligation by particles does not inhibit LPS-induced pro-IL-1β and TNF-α production.

We further addressed whether PS stimulate macrophages to produce ROS and NO. Consistent with previous reports (Shi et al., 2016; Wink et al., 2011), IFN-γ or Nigericin induced macrophage NO or ROS production, respectively; however, PS induced neither NO nor ROS (Figs. S6 and

Fig. 3. Tim4 binds PS via aromatic-aromatic interactions. A. Model of aromatic-aromatic interactions between Tim4 and surface of multi-wall carbon nanotubes (MWCNTs) or PS. Tim4 extracellular IgV domain (PBD ID: 3bi9) harbors an aromatic cluster consisting of F120 and W119 highlighted with red. B. Indicated NIH-3T3 cells were stained with PE-cIg (black histograms) or PE-anti-Tim4 (red histograms). The expression of wild-type (WT) Tim4 and the WF119/120AA mutant on NIH-3T3 cells was analyzed by flow cytometry. C. Indicated NIH-3T3 cells were treated with (dark histograms) or without (white histograms) 100 or 300 μg/ml of 0.8 μm PS particles for 30 min. PS binding was analyzed as in Fig. 1B. Numbers indicate MSI. D. Indicated NIH-3T3 cells were treated with different doses of PS or MWCNTs for 30 min. Particle recognition was analyzed as in C. The ΔMSI was calculated as in Fig. 1C. Data are shown as individual value (dots), mean (columns), and SD (error bars) from n = 3. $^{**}p < 0.01$, two-way ANOVA. E. Indicated NIH-3T3 cells cultured as in C were stained with Alexa Fluor (AF) 594-phalloidin and DAPI. Cells were analyzed by fluorescence microscopy. White bars indicate 20 μm. (For interpretation of the references to color in this figure legend, the reader is referred to the web version of this article.)

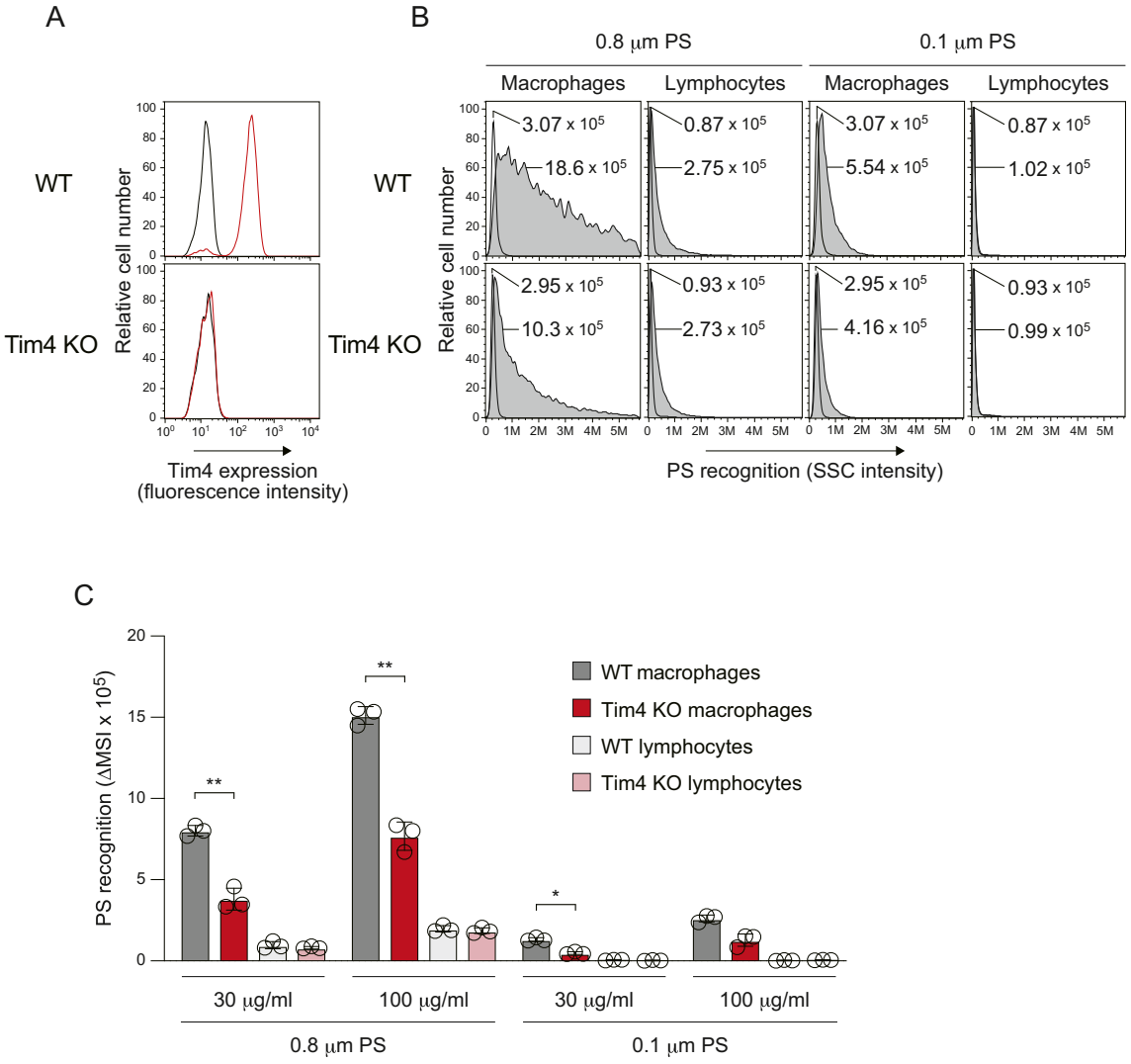

Fig. 5. Macrophages use Tim4 for PS recognition. A. WT and Tim4 knockout (KO) mouse peritoneal resident cells were stained with FITC-anti-CD11b and PE-cIg (black histograms) and PE-anti-Tim4 (red histograms). Tim4 expression on CD11b-high macrophages was analyzed by flow cytometry. See also Fig. S3. B. Peritoneal resident cells were treated with 0.8 or 0.1 μm diameter PS particles (100 μg/ml each) for 30 min. PS recognition by CD11b-high macrophages or by CD11b-low/negative lymphocytes was analyzed as in Fig. 2B. Numbers indicate MSI. C. Macrophage recognition of the indicated size and dose of PS particles was analyzed as in B. The ΔMSI was calculated as in Fig. 1C. Data are shown individual value (dots), mean (columns), and SD (error bars) from $n = 3$. $^*p < 0.05$, $^{**}p < 0.01$, two-way ANOVA. (For interpretation of the references to color in this figure legend, the reader is referred to the web version of this article.)

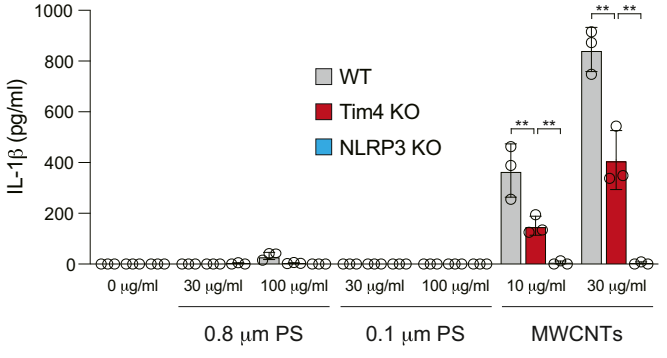

Fig. 6. IL-1β secretion from mouse peritoneal cells. WT, Tim4 KO, and NLRP3 KO mouse peritoneal cells were primed with 3 ng/ml of lipopolysaccharide (LPS) for 3 h and were then stimulated with the indicated dose of particles or fibers for 4 h. IL-1β in cell culture supernatants was measured by ELISA. Data are shown individual value (dots), mean (columns), and SD (error bars) from n = 3. **p < 0.01, two-way ANOVA. See also Fig. S4.

S7). Taken together, these data suggest that although PS particles are engulfed by mouse macrophages via Tim4, PS particles only negligibly induce inflammation.

3.3. PS microplastics interfere with Tim4-mediated efferocytosis

Because Tim4 PtdSer binding site contains PS binding site (Fig. 3), we finally addressed whether PS microplastics interfere with efferocytosis. To measure efferocytosis, we used UV-irradiated apoptotic mouse thymocytes labeled with a pH-sensitive cyanine dye, CypHer5e. WT mouse macrophages engulfing apoptotic cells became CypHer5e-positive, and the fluorescence intensity was decreased in Tim4 KO macrophages (Fig. 7A, B), indicating that Tim4 is essential for efferocytosis. Importantly, 0.8 μm PS particles inhibited efferocytosis, while 0.1 μm PS particles did not (data not shown). Although the underlying reason for this is unknown, particle size may impact the inhibition of efferocytosis. These results suggest that a certain size of PS microplastics may perturb Tim4 recognition of apoptotic cells.

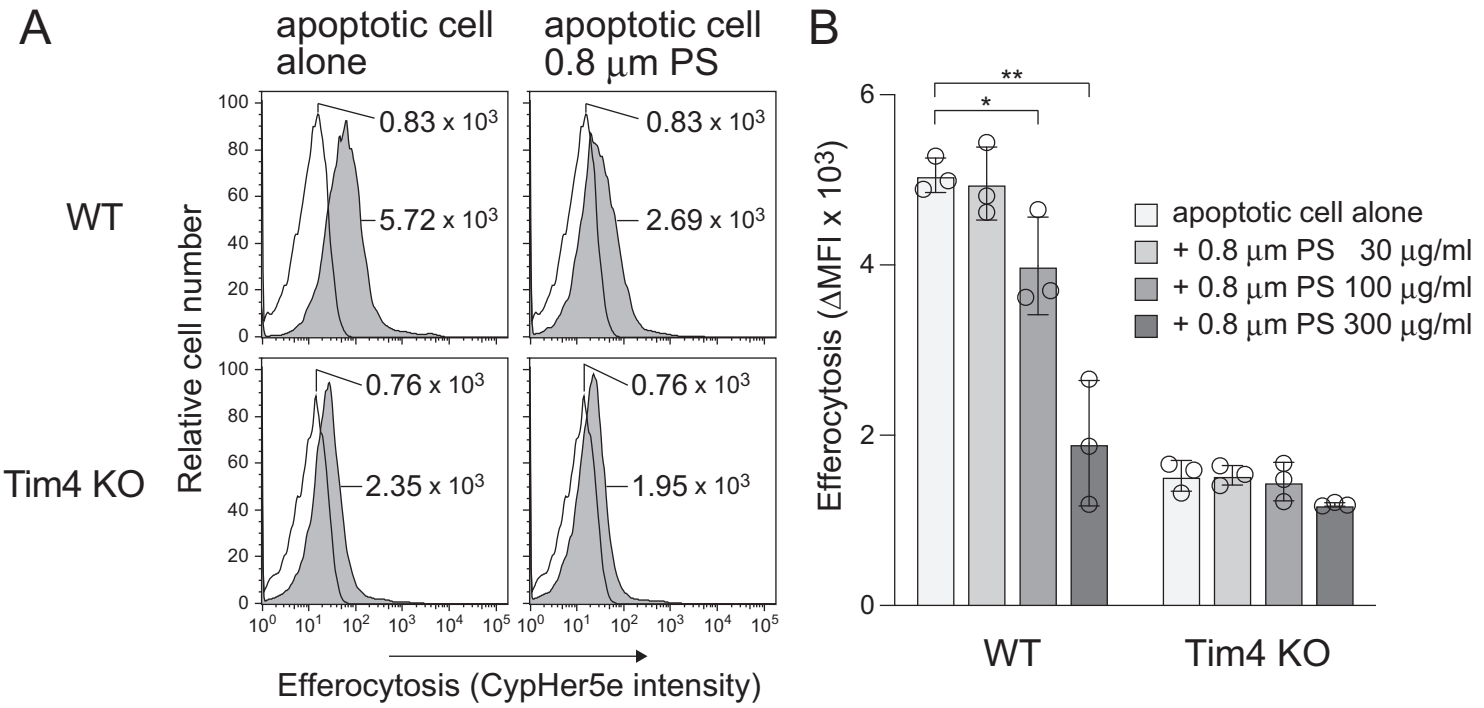

Fig. 7. PS particles perturb efferocytosis. A. WT and Tim4 KO mouse peritoneal cells were pretreated with or without 0.8 μm diameter PS particles (300 μg/ml) for 30 min and then were treated with CypHer5e-labeled apoptotic cells for 30 min (dark histograms). Cells were the stained with FITC-anti-CD11b, and efferocytosis by CD11b-high macrophages was analyzed by flow cytometry. White histograms indicate untreated macrophages. Numbers indicate MFI of CypHer5e. B. Efferocytosis was analyzed as in A. The ΔMFI was calculated as in Fig. 1C. Data are shown as individual value (dots), mean (columns), and SD (error bars) from n = 3. *$p < 0.05$, **$p < 0.01$, two-way ANOVA.

4. Discussion

Macrophages recognize pathogen-associated molecular patterns (PAMPs) through pattern-recognition receptors (PRRs) (Takeuchi and Akira, 2010). Besides pathogens, macrophages efficiently recognize environmental particles and nanomaterials; nevertheless, it is not fully understood how macrophages recognize such inorganic particles (Nakayama, 2018; Rashidi et al., 2020). In this context, we have recently found that class B scavenger receptors SR-B1 and CD36 recognize silica in a charge-dependent manner (Tsugita et al., 2017). Regarding the recognition of carbon nanomaterials, we found that Tim4, but not class B scavenger receptors, binds MWCNTs and carbon black nanoparticles (CBNPs) via aromatic-aromatic interactions (Omori et al., 2021). Likewise, here we show that Tim4 binds PS particles, highlighting a novel interface between microplastics and biological systems through aromatic-aromatic interactions. Thus, we propose that through their surface receptors macrophages discriminate not only between microbes, but also between particulates.

Some environmental particles are efficiently engulfed by macrophages and cause NLRP3-dependent IL-1β secretion (Franklin et al., 2016; Rashidi et al., 2020; Swanson et al., 2019). NLRP3 inflammasome activation requires at least two signals. The first is mediated by PAMPs or cytokines that trigger nuclear factor κB (NF-κB)-mediated upregulation of NLRP3 along with pro-IL-1β. The second signal stimulates assembly a complex of multiple proteins including NLRP3, ASC, and pro-caspase-1 to activate caspase-1 that processes pro-IL-1β to mature IL-1β. In contrast to IL-1β, the secretion of TNF-α, IL-6, and IL-10 is induced by signal 1 alone (Franklin et al., 2016; Rashidi et al., 2020; Swanson et al., 2019). Although environmental particles containing PAMPs such as LPS may transmit both signal 1 and signal 2, pristine particles per se could stimulate only signal 2 via phagosome damage. Whether particles stimulate signal 2 or not may depend on their size and shape. For instance, MWCNTs as well as CBNPs are recognized and engulfed by macrophages via Tim4; however, only the former has a rigid needle-like structure and causes phagosome damage leading to pyroptosis and NLRP3 inflammasome activation, resulting in inflammation (Omori et al., 2021). Here we show that PS particles as well as CBNPs are microspheres and thus do not markedly transmit signal 2. It has been reported that signal 1 and signal 2 also induce NO and ROS, respectively (Shi et al., 2016; Wink et al., 2011); however, PS particles induced neither NO nor ROS production. These data support the idea that size and shape impact particle toxicity (Donaldson et al., 2010). It has been reported that overexpression of Tim4 inhibits LPS-mediated signal 1 (Xu et al., 2015). Although we did not observe the inhibitory effect of MWCNTs and PS particles on LPS-induced cytokine production, Tim4 ligation by particles may inhibit LPS-induced inflammation under certain conditions.

Efferocytosis plays an important role in maintenance of tissue homeostasis. Impaired efferocytosis is likely associated with inflammation and autoimmune disease (Doran et al., 2020; Nagata, 2018). Indeed, masking of Tim4 by anti-Tim4 neutralizing mAb drastically inhibits efferocytosis and induces autoantibody production in mice (Miyanishi et al., 2007). Tim4 recognizes PtdSer on apoptotic cells via the metal-ion dependent ligand binding site (MILIBS) consisting of four amino acid residues: Trp119-Phe120-Asn121-Asp122 (Kobayashi et al., 2007; Santiago et al., 2007), which includes an aromatic cluster (Trp119-Phe120) that is essential for PS binding. Thus, PS microplastics may compete with apoptotic cells for Tim4 binding. It is unlikely that PS microplastics cause acute toxicity; however, chronic exposure of large amounts of these particles may perturb efferocytosis, causing chronic inflammation and autoimmune diseases (Doran et al., 2020; Nagata, 2018).

In conclusion, this study demonstrates that Tim4 recognizes PS microparticles via its extracellular aromatic cluster, highlighting a novel interface between microplastics and biological systems. Although the PS microparticles used in this study did not cause macrophage inflammatory responses, environmental plastics may contain nano-sized and/or fibrous particles and may adsorb PAMPs and/or polycyclic aromatic hydrocarbons which can cause acute inflammation and/or cancer (Wheeler et al., 2021). In this context, measurement of the size and shape of plastic particles in complex environmental samples has just begun (Mitrano et al., 2021). Although it is widely accepted that humans are exposed to microplastics, the environmentally relevant dose remains uncertain (Amato-Lourenco et al., 2020; Mohamed Nor et al., 2021; Wright and Kelly, 2017). Given that cellular uptake of microplastics is a key process for their potential toxicity, identification of Tim4 as a receptor recognizing PS particles may provide better understanding of absorption, distribution, excretion, and toxicity of PS plastics.

CRediT authorship contribution statement

Miki Kuroiwa: experimental work; data analysis. **Shinichiro Yamaguchi:** experimental work; data analysis. **Yoshinobu Kato:** experimental work. **Arisa Hori:** experimental work. **Saori Toyoura:** experimental work. **Mai Nakahara:** experimental work. **Nobuyuki Morimoto:** experimental work; data analysis; writing. **Masafumi Nakayama:** conceptualization and design; experimental work; writing.

Data availability

Data will be made available on request.

Declaration of competing interest

The authors declare that they have no known competing financial interests or personal relationships that could have appeared to influence the work reported in this paper.

Acknowledgements

We thank Keiko Furuta (Division of Electron Microscopic Study, Center for Anatomical Studies, Graduate School of Medicine, Kyoto University) for technical assistance in electron microscopy. We also thank Professor Shigekazu Nagata (Osaka University) for Tim4 KO mice. This work was supported by Japan Society for the Promotion of Sciences (JSPS) under grant # JP22H03340 to M.N., # JP22H03969 to N.M., and the Naito Foundation to M.N.

Appendix A. Supplementary data

Supplementary data to this article can be found online at https://doi.org/10.1016/j.scitotenv.2023.162586.

References

Amato-Lourenco, L.F., Dos Santos Galvao, L., de Weger, L.A., Hiemstra, P.S., Vijver, M.G., Mauad, T., 2020. An emerging class of air pollutants: potential effects of microplastics to respiratory human health? Sci. Total Environ. 749, 141676.

Andrady, A.L., 2011. Microplastics in the marine environment. Mar. Pollut. Bull. 62, 1596–1605.

Areschoug, T., Gordon, S., 2009. Scavenger receptors: role in innate immunity and microbial pathogenesis. Cell. Microbiol. 11, 1160–1169.

Arredouani, M., Yang, Z., Ning, Y., Qin, G., Soininen, R., Tryggvason, K., Kobzik, L., 2004. The scavenger receptor MARCO is required for lung defense against pneumococcal pneumonia and inhaled particles. J. Exp. Med. 200, 267–272.

Cozar, A., Echevarria, F., Gonzalez-Gordillo, J.I., Irigoien, X., Ubeda, B., Hernandez-Leon, S., Palma, A.T., Navarro, S., Garcia-de-Lomas, J., Ruiz, A., et al., 2014. Plastic debris in the open ocean. Proc. Natl. Acad. Sci. U. S. A. 111, 10239–10244.

Donaldson, K., Murphy, F.A., Duffin, R., Poland, C.A., 2010. Asbestos, carbon nanotubes and the pleural mesothelium: a review of the hypothesis regarding the role of long fibre retention in the parietal pleura, inflammation and mesothelioma. Part Fibre Toxicol 7, 5.

Doran, A.C., Yurdagul Jr., A., Tabas, I., 2020. Efferocytosis in health and disease. Nat. Rev. Immunol. 20, 254–267.

Franklin, B.S., Mangan, M.S., Latz, E., 2016. Crystal formation in inflammation. Annu. Rev. Immunol. 34, 173–202.

Guo, H.L., Zhao, X.P., 2004. Preparation of a kind of red encapsulated electrophoretic ink. Opt. Mater. 26, 297–300.

Heppleston, A.G., 1984. Pulmonary toxicology of silica, coal and asbestos. Environ. Health Perspect. 55, 111–127.
Horvatits, T., Tamminga, M., Liu, B., Sebode, M., Carambia, A., Fischer, L., Puschel, K., Huber, S., Fischer, E.K., 2022. Microplastics detected in cirrhotic liver tissue. EBioMedicine 82, 104147.
Jang, M., Shim, W.J., Han, G.M., Rani, M., Song, Y.K., Hong, S.H., 2017. Widespread detection of a brominated flame retardant, hexabromocyclododecane, in expanded polystyrene marine debris and microplastics from South Korea and the Asia-Pacific coastal region. Environ. Pollut. 231, 785–794.
Jeon, S., Lee, D.K., Jeong, J., Yang, S.I., Kim, J.S., Kim, J., Cho, W.S., 2021. The reactive oxygen species as pathogenic factors of fragmented microplastics to macrophages. Environ. Pollut. 281, 117006.
Kanno, S., Furuyama, A., Hirano, S., 2007. A murine scavenger receptor MARCO recognizes polystyrene nanoparticles. Toxicol. Sci. 97, 398–406.
Kitamura, T., Koshino, Y., Shibata, F., Oki, T., Nakajima, H., Nosaka, T., Kumagai, H., 2003. Retrovirus-mediated gene transfer and expression cloning: powerful tools in functional genomics. Exp. Hematol. 31, 1007–1014.
Kobayashi, N., Karisola, P., Pena-Cruz, V., Dorfman, D.M., Jinushi, M., Umetsu, S.E., Butte, M.J., Nagumo, H., Chernova, I., Zhu, B., et al., 2007. TIM-1 and TIM-4 glycoproteins bind phosphatidylserine and mediate uptake of apoptotic cells. Immunity 27, 927–940.
Koelmans, A.A., Redondo-Hasselerharm, P.E., Nor, N.H.M., de Ruijter, V.N., Mintenig, S.M., Kooi, M., 2022. Risk assessment of microplastic particles. Nat. Rev. Mater. 7, 138–152.
Kovarova, M., Hesker, P.R., Jania, L., Nguyen, M., Snouwaert, J.N., Xiang, Z., Lommatzsch, S.E., Huang, M.T., Ting, J.P., Koller, B.H., 2012. NLRP1-dependent pyroptosis leads to acute lung injury and morbidity in mice. J. Immunol. 189, 2006–2016.
Leslie, H.A., van Velzen, M.J.M., Brandsma, S.H., Vethaak, A.D., Garcia-Vallejo, J.J., Lamoree, M.H., 2022. Discovery and quantification of plastic particle pollution in human blood. Environ. Int. 163, 107199.
Leung, C.C., Yu, I.T., Chen, W., 2012. Silicosis. Lancet 379, 2008–2018.
MacLeod, M., Arp, H.P.H., Tekman, M.B., Jahnke, A., 2021. The global threat from plastic pollution. Science 373, 61–65.
Merkley, S.D., Moss, H.C., Goodfellow, S.M., Ling, C.L., Meyer-Hagen, J.L., Weaver, J., Campen, M.J., Castillo, E.F., 2022. Polystyrene microplastics induce an immunometabolic active state in macrophages. Cell Biol. Toxicol. 38, 31–41.
Mitrano, D.M., Wick, P., Nowack, B., 2021. Placing nanoplastics in the context of global plastic pollution. Nat. Nanotechnol. 16, 491–500.
Miyanishi, M., Segawa, K., Nagata, S., 2012. Synergistic effect of Tim4 and MFG-E8 null mutations on the development of autoimmunity. Int. Immunol. 24, 551–559.
Miyanishi, M., Tada, K., Koike, M., Uchiyama, Y., Kitamura, T., Nagata, S., 2007. Identification of Tim4 as a phosphatidylserine receptor. Nature 450, 435–439.
Mohamed Nor, N.H., Kooi, M., Diepens, N.J., Koelmans, A.A., 2021. Lifetime accumulation of microplastic in children and adults. Environ Sci Technol 55, 5084–5096.
Nagata, S., 2018. Apoptosis and clearance of apoptotic cells. Annu. Rev. Immunol. 36, 489–517.
Nakayama, M., 2018. Macrophage recognition of crystals and nanoparticles. Front. Immunol. 9, 103.
Nakayama, M., Akiba, H., Takeda, K., Kojima, Y., Hashiguchi, M., Azuma, M., Yagita, H., Okumura, K., 2009. Tim-3 mediates phagocytosis of apoptotic cells and cross-presentation. Blood 113, 3821–3830.
Omori, S., Tsugita, M., Hoshikawa, Y., Morita, M., Ito, F., Yamaguchi, S.I., Xie, Q., Noyori, O., Yamaguchi, T., Takada, A., et al., 2021. Tim4 recognizes carbon nanotubes and mediates phagocytosis leading to granuloma formation. Cell Rep. 34, 108734.
Prata, J.C., 2018. Airborne microplastics: consequences to human health? Environ. Pollut. 234, 115–126.
Prata, J.C., da Costa, J.P., Lopes, I., Duarte, A.C., Rocha-Santos, T., 2020. Environmental exposure to microplastics: an overview on possible human health effects. Sci. Total Environ. 702, 134455.
Ramsperger, A., Narayana, V.K.B., Gross, W., Mohanraj, J., Thelakkat, M., Greiner, A., Schmalz, H., Kress, H., Laforsch, C., 2020. Environmental exposure enhances the internalization of microplastic particles into cells. Sci. Adv. 6.
Rashidi, M., Wicks, I.P., Vince, J.E., 2020. Inflammasomes and cell death: common pathways in microparticle diseases. Trends Mol. Med. 26, 1003–1020.
Santiago, C., Ballesteros, A., Martinez-Munoz, L., Mellado, M., Kaplan, G.G., Freeman, G.J., Casasnovas, J.M., 2007. Structures of T cell immunoglobulin mucin protein 4 show a metal-ion-dependent ligand binding site where phosphatidylserine binds. Immunity 27, 941–951.
Shi, H., Wang, Y., Li, X., Zhan, X., Tang, M., Fina, M., Su, L., Pratt, D., Bu, C.H., Hildebrand, S., et al., 2016. NLRP3 activation and mitosis are mutually exclusive events coordinated by NEK7, a new inflammasome component. Nat. Immunol. 17, 250–258.
Shi, Q.Y., Tang, J.C., Liu, R.T., Wang, L., 2022. Toxicity in vitro reveals potential impacts of microplastics and nanoplastics on human health: a review. Crit. Rev. Environ. Sci. Technol. 52, 3863–3895.
Stubbins, A., Law, K.L., Munoz, S.E., Bianchi, T.S., Zhu, L., 2021. Plastics in the earth system. Science 373, 51–55.
Swanson, K.V., Deng, M., Ting, J.P., 2019. The NLRP3 inflammasome: molecular activation and regulation to therapeutics. Nat. Rev. Immunol. 19, 477–489.
Takeuchi, O., Akira, S., 2010. Pattern recognition receptors and inflammation. Cell 140, 805–820.
Tsugita, M., Morimoto, N., Tashiro, M., Kinoshita, K., Nakayama, M., 2017. SR-B1 is a silica receptor that mediates canonical inflammasome activation. Cell Rep. 18, 1298–1311.
Vethaak, A.D., Legler, J., 2021. Microplastics and human health. Science 371, 672–674.
Wheeler, K.E., Chetwynd, A.J., Fahy, K.M., Hong, B.S., Tochihuitl, J.A., Foster, L.A., Lynch, I., 2021. Environmental dimensions of the protein corona. Nat. Nanotechnol. 16, 617–629.
Wink, D.A., Hines, H.B., Cheng, R.Y., Switzer, C.H., Flores-Santana, W., Vitek, M.P., Ridnour, L.A., Colton, C.A., 2011. Nitric oxide and redox mechanisms in the immune response. J. Leukoc. Biol. 89, 873–891.
Wright, S.L., Kelly, F.J., 2017. Plastic and human health: a micro Issue? Environ Sci Technol 51, 6634–6647.
Xu, L.Y., Qi, J.N., Liu, X., Ma, H.X., Yuan, W., Zhao, P.Q., Liang, X.H., Xu, Y., Wang, H.X., Xu, X.Y., et al., 2015. Tim-4 inhibits NO generation by murine macrophages. PLoS One 10, e0124771.